Two-neutron transfer analysis of the $^{16}O(^{18}O,^{16}O)^{18}O$ reaction

M. J. Ermamatov,[1,2] F. Cappuzzello,[3,4] J. Lubian,[1] M. Cubero,[5] C. Agodi,[3] D. Carbone,[3] M. Cavallaro,[3] J. L. Ferreira,[1] A. Foti,[4,6] V. N. Garcia,[7] A. Gargano,[8] J. A. Lay,[9,10] S. M. Lenzi,[9,10] R. Linares,[1] G. Santagati,[3] and A. Vitturi[9,10]

[1]*Instituto de Física, Universidade Federal Fluminense, 24210-340, Niterói, Rio de Janeiro, Brazil*

[2]*Institute of Nuclear Physics, Ulughbek, Tashkent 100214, Uzbekistan*

[3]*INFN, Laboratori Nazionali del Sud, I-95125 Catania, Italy*

[4]*Dipartimento di Fisica e Astronomia, Università di Catania, I-95125 Catania, Italy*

[5]*CICANUM, Universidad de Costa Rica, 11502 Apartado 2060 San José, Costa Rica*

[6]*INFN, Sezione di Catania, I-95125 Catania, Italy*

[7]*Instituto Federal de Educação, Ciência e Tecnologia Fluminense, Campos Centro, 28030-131, Campos dos Goytacazes, Rio de Janeiro, Brazil*

[8]*Istituto Nazionale di Fisica Nucleare, Sezione di Napoli, Napoli, Italy*

[9]*Dipartimento di Fisica e Astronomia Galileo Galilei, Università di Padova, via Marzolo 8, I-35131 Padova, Italy*

[10]*INFN, Sezione di Padova, via Marzolo 8, I-35131 Padova, Italy*

(Received 20 April 2016; revised manuscript received 8 July 2016; published 12 August 2016)

Recently a quantitative description of the two-neutron transfer reaction $^{12}C(^{18}O,^{16}O)^{14}C$ was performed and the measured cross sections were successfully reproduced [M. Cavallaro *et al.*, Phys. Rev. C **88**, 054601 (2013)]. This task was accomplished by combining nuclear structure calculations of spectroscopic amplitudes and a full quantum description of the reaction mechanism. Verification of such a theoretical approach to other heavy nuclear systems is mandatory in order to use $(^{18}O,^{16}O)$ reactions to assess pair configurations in nuclear states. In this work we apply this methodology to the $^{16}O(^{18}O,^{16}O)^{18}O$ reaction at 84 MeV. Experimental angular distributions for the two-neutron transfer to the ground state and 2_1^+ state of ^{18}O were obtained using the MAGNEX spectrometer at INFN-LNS. The roles of one- and two-step processes are analyzed under the exact finite range coupled reaction channel and the second order distorted wave Born approximation. We conclude that the one-step transfer mechanism is dominant in this system.

I. INTRODUCTION

The atomic nucleus is a complex many-body system built up from fundamental nucleon-nucleon interactions. The nuclear structure exhibits striking features like collective and single-particle states, pairing correlations, clustering, and more [1,2]. Knowledge of relevant internal degrees of freedom is important to understand the stability of nuclei, especially outside the stability valley. Such information can be extracted from direct nuclear reactions like elastic and inelastic scatterings, nucleon transfer reactions, etc.

In particular, transfer reactions, in which the projectile transfers one or more nucleons to or from the target nucleus, provide access to nuclear spectroscopic amplitudes. Reactions with light ions like (p,t) and (t,p) have been extensively used to study pairing correlations in proton-rich and neutron-rich nuclei, respectively [3–13]. Such types of reactions are advantageous because, from the experimental point of view, detection of light particles provides good energy resolution and clear particle identification. From the theoretical side, analysis usually does not require complicated coupling schemes and the reactions can be described using the second order distorted wave Born approximation (DWBA) approach [14–17]. However, nowadays, the use of triton beams is strongly limited due to radiation safety. Other light neutron-rich projectiles like ^{6}He, ^{8}Li, and ^{10}Be are exotic nuclei and therefore beam intensities are usually too low for measurements of nuclear reactions involving transfer of nucleons.

Within this scenario, the (^{18}O, ^{16}O) reaction is a promising option. However, the reaction may proceed through many intermediate excited states so that the number of possible paths can be large. In addition, one of the difficulties consists of the coupling of the initial and final states with inelastic excitations, which opens alternative routes for the reaction. Coupled channel corrections are necessary to explain, for example, the anomalous behavior of the angular distributions observed in the transitions to the 2^+ vibrational states in medium mass nuclei [18,19]. The coupled reaction channel (CRC) is the best suited approach to interpret the data. In such calculations the spectroscopic amplitudes of the nuclear states are crucial. However, an additional scaling factor has to be introduced to reproduce the magnitude of the angular cross section angular distributions.

Recently, the potentiality of spectroscopic studies with heavy-ion projectiles was demonstrated in the (^{18}O, ^{16}O) reaction on light nuclei [20–22]. The methodology is based on a combination of shell-model and direct nuclear reaction calculations. The first is applied to obtain reliable spectroscopic amplitudes to be used as input in the calculations of cross sections. Within this approach, the experimental cross sections for the two-neutron transfer were reproduced, for the first time, without any scaling factor [23]. Also demonstrated was the dominance of the one-step (direct) over the two-step (sequential) process. An independent study was performed in the $^{206}Pb(^{18}O,^{16}O)^{208}Pb$ reaction at 79 MeV [24]. Again, theoretical analysis agrees with the experimental angular

distributions and shows that the direct transfer is the main mechanism. In both works, target nuclei were closed shell.

In a further step along the analysis of two-neutron transfer reactions with nuclei around a closed shell, we show in this work the analysis of the ^{16}O(^{18}O,^{16}O)^{18}O reaction at 84 MeV. In this particular system we perform shell-model calculations with two effective interactions: the Zuker-Buck-McGrory (ZBM) [25] and the psdmod [26], as referred in the NUSHELL code. The former, which assumes a $1p_{1/2}$, $1d_{5/2}$, $2s_{1/2}$ smaller valence space, was also used in Ref. [23]. The latter is a modified version of the PSDWBT interaction [26], defined in the $1p_{3/2}$, $1p_{1/2}$, $1d_{5/2}$, $2s_{1/2}$, $1d_{3/2}$ space. PSDWBT stands for the modification performed by Warburton and Brown to the p-sd part of the interaction PSDT [27], concerning to the p-sd shells. The psdmod allows one to investigate the effects of the $1p_{3/2}$ and $1d_{3/2}$ orbitals, not included in the ZBM.

The paper is organized as follows: the experimental procedure is discussed in Sec. II, the theoretical approach, used for the nuclear-structure and direct reaction calculations, is discussed in Sec. III, and the conclusions are drawn in Sec. IV.

II. EXPERIMENTAL RESULTS

The experiment was performed at the Istituto Nazionale di Fisica Nucleare, Laboratori Nazionali del Sud in Catania. An 84-MeV $^{18}O^{6+}$ beam was accelerated towards a target composed of 212 μg/cm^2 WO_3 film deposited on 193 μg/cm^2 Au backing. The reaction products were momentum analyzed by the MAGNEX large acceptance spectrometer [28–30] and detected by the hybrid focal plane detector (FPD) composed of a gas section and solid state detectors [31,32]. The FPD measures all relevant parameters (positions, angles, energy loss, and residual energy) for particle identification and trajectory reconstruction. Details of the data reduction technique are described in Refs. [32–35].

The experiment was performed at two angular settings, with the spectrometer optical axis centered at $\theta_{opt} = 8^\circ$ and 10° and the aperture diaphragms in the full open mode. This corresponds to accepting ejectiles scattered in the range of angles in the laboratory frame $3^\circ \lesssim \theta_{lab} \lesssim 14^\circ$ and $5^\circ \lesssim \theta_{lab} \lesssim 16^\circ$, respectively, and provides a fairly wide angular overlap between the two settings. Overall resolution of 250 keV [full width at half maximum (FWHM)] in energy and 0.3° in angle was obtained in the laboratory frame after trajectory reconstruction of the data. Energy straggling in the target contributes with about 100 keV, estimated by the SRIM code [36], while kinematic broadening within the angular bin is about 200 keV.

Figure 1 shows a typical energy spectrum for the angular range between 5.5° and 6.5° in the laboratory frame. The energy axis is referred to the ^{18}O excitation energy $E_x = Q_0 - Q$, where Q_0 is the reaction Q-value for the ground state to ground state transition (g.s. $\rightarrow$ g.s.). Several sharp peaks are observed, indicating a relevant population of bound and low-lying resonant states. The continuum background observed at excitation energies higher than the neutron separation energy ($S_n = 8.04$ MeV) is due to the three-body kinematics connected to the one-neutron emission.

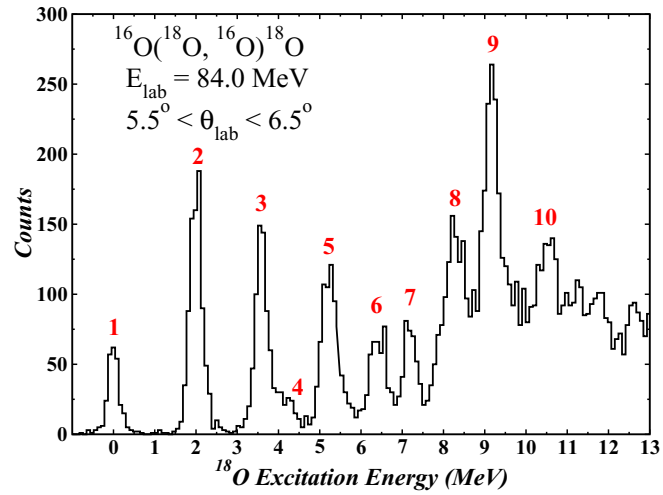


FIG. 1. Energy spectra for the angular range between 5.5° and 6.5° in the laboratory frame. Peaks are numerically labeled as reported in Table I.

The identification of the main peaks was performed by comparing our spectrum with the spectrum of the ^{16}O(t,p)^{18}O reaction [37] as listed in Table I. The ground state and the first excited state (peaks 1 and 2, respectively) are clearly separated. The third peak corresponds to unresolved 4^+, 0^+, and 2^+ states. The same holds for peaks 5 and 6, which correspond to the superposition of many states. Peak 4, a 1^- state at 4.46 MeV, is highly suppressed as compared to the intensity observed in the (t,p) reaction. It is worth noticing that narrow resonances between one- and two-neutron separation energy are strongly populated by this (^{18}O,^{16}O) reaction. This resembles the case

TABLE I. States populated in the ^{16}O(^{18}O,^{16}O)^{18}O reaction at 84 MeV (see Fig. 1).

Label	Energy (MeV)	J^π
1	0.00	0^+
2	1.98	2^+
3	3.55 3.63 3.92	
4	4.46	1^-
5	5.10 5.26 5.34 5.38 5.53	
6	6.20 6.35 6.40 6.88	
7	7.12	4^+
8	8.28[a]	3^-
9	9.03[a]	
10	10.40[a] 10.61[a]	

[a]The most intense states according to (t,p) reaction [37] were considered.

of ^{14}C where this class of resonances was attributed to states with two-neutron plus core dominant configuration [21,23]. Above the neutron separation energy the density of states is high. Therefore, in Table I we indicate the energies of the more intense states according to the (t,p) reaction on ^{16}O. Lorentzian fits for peaks 8, 9, and 10 of Table I and Fig. 1 gave FWHM of 0.55, 0.35, and 0.44 MeV, respectively.

In our experimental setup the ^{16}O ejectiles may also be generated in the two-neutron stripping reactions on ^{184}W or ^{197}Au, both present in the target. The (^{18}O,^{16}O) reactions from different target nuclei have a kinematically distinct behavior that becomes apparent in a $\theta_{\rm lab}$-E plot. In previous work this expedient was exploited to identify contaminants in the target (see Fig. 5 in Ref. [38]). Considering the g.s. $\rightarrow$ g.s. transfer channel for both ^{184}W and ^{197}Au, the ^{16}O$_{\rm g.s.}$ ejectiles have higher kinetic energies than the ones we are interested in. Therefore, those ejectiles in the ^{18}O experimental spectrum represented in Fig. 1 lie in the negative region. Very few ^{16}O particles were observed in this region, indicating a negligible amount of such background. A major interference to be concerned with is the elastic scattering of ^{18}O + ^{16}O at backward angles, which contributes with ^{16}O recoiling particles at forward angles that are kinematically indistinguishable from the ejectiles in the g.s. $\rightarrow$ g.s. two-neutron transfer channel. The interference due to the elastic channel on the two-neutron angular distributions is discussed in detail in the next section.

III. THEORETICAL ANALYSIS

It is well known that for pure *heavy-ion* elastic scattering the cross section typically decreases smoothly as the angle increases and that in reactions involving similar nuclei a contamination due to the elastic transfer appears at backward angles in the elastic scattering cross section and correspondingly at forward angles for elastic transfer cross sections [39,40]. This is due to the fact that in the experiment the elastic scattering of a projectile at a given θ is indistinguishable from the elastic transfer at the angle $180^\circ - \theta$. The interference of the two contributions can give rise to oscillatory patterns, more or less significant depending on the considered angle and bombarding energy. This behavior is confirmed also by experiments, including ^{18}O+^{16}O collisions at lower energies than in the present study [39].

To check the situation in our case, we performed a calculation that accounts for the interference of the two processes. A simple potential with the parametrization of Akyuz and Winther [41] for the real part (and an imaginary part with same geometry and half the strength) was used for the "pure elastic" channel. Leaving for the rest of the paper a more accurate description of the process, a macroscopic form factor $F(r) = \beta_{\rm p}\frac{dU}{dA} = \frac{\beta_{\rm p}}{3A}\frac{dU}{dr}$ was used for the two-particle transfer channel, with a pairing deformation parameter $\beta_{\rm p}$ adjusted to fit the magnitude of the cross section ($\beta_{\rm p} = 4$). The quantal interference is obtained along the procedure illustrated in Ref. [39], adding to the potential an exchange parity-dependent term equivalent to the transfer form factor. This procedure allows one to properly calculate the interference in a full quantum model, which is reduced to the solution of

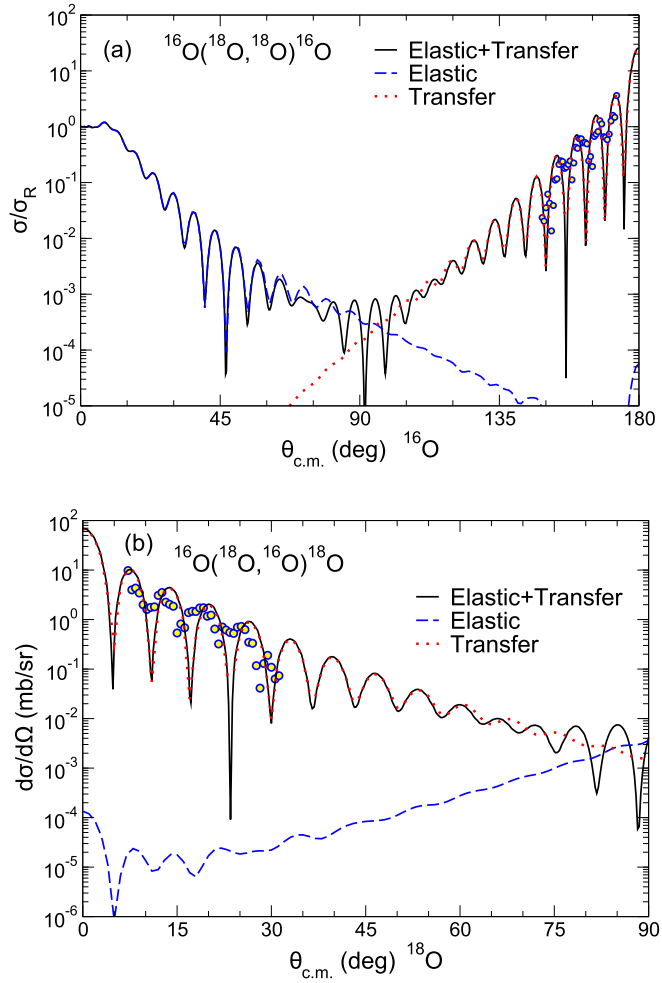


FIG. 2. Estimation of the effect of elastic cross section by simple macroscopic calculation of (a) the final ^{16}O and (b) the complementary ^{18}O channels cross sections.

the Schrödinger equation with a particular parity-dependent optical potential. The results are shown in Fig. 2(a) for the final ^{16}O channel (in terms of ratio to Rutherford) and equivalently in Fig. 2(b) for the complementary ^{18}O channel. In both figures the dashed line refers to the "pure" elastic contribution, the dotted line refers to the "pure" transfer, and the solid line includes the interference of the two processes. As the figure clearly shows, at this bombarding energy the interference is significant only around 90°, while the measured events in the forward ^{18}O angles can be safely attributed to the genuine elastic transfer process.

We performed prior exact finite-range CRC and two-step DWBA calculations for two-neutron transfer reactions, using the FRESCO code [42]. Nonorthogonality corrections and full complex remnant terms were used in the coupling scheme. Only the transition terms to the ^{18}O ground and first excited 2^+ state were analyzed, since the other populated states are not resolved in the energy spectra. In these calculations we used the São Paulo double folding potential [43] as the optical potential. In the entrance partition a strength coefficient of 0.6 for the imaginary part of the optical potential was used to account for dissipative processes and also for the missing couplings to

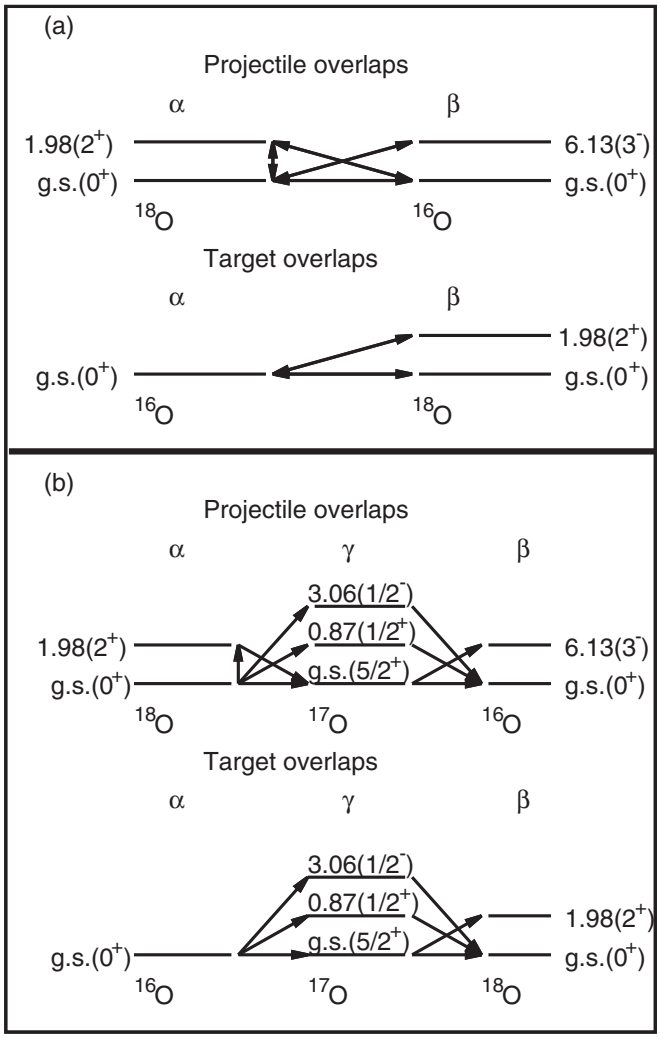


FIG. 3. Coupling for (a) direct CRC and (b) two-step DWBA transfers.

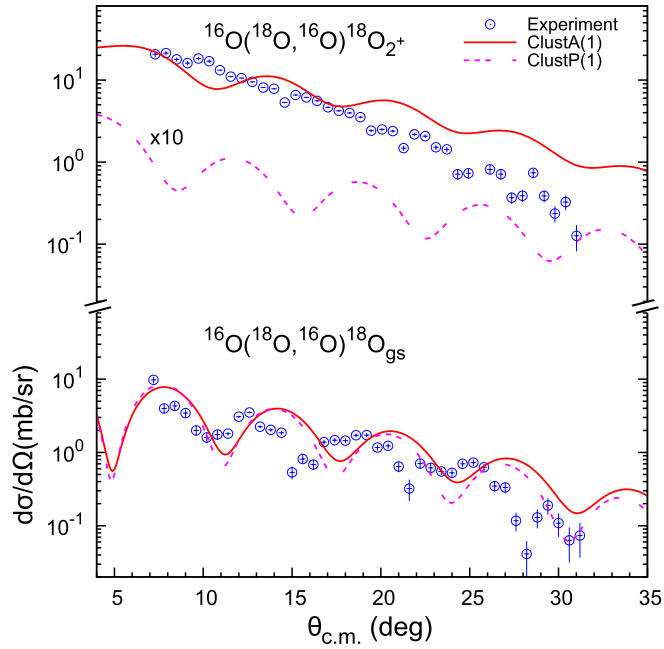


FIG. 4. Comparison of angular distributions in the cluster model in the case of the spin antiparallel [ClustA(1)] and parallel [ClustP(1)] transfer with the experimental data for the ^{16}O(^{18}O,^{16}O)^{18}O$_{gs}$ (bottom) and ^{16}O(^{18}O,^{16}O)^{18}O$_{2^+}$ (top) channels. The value of the spectroscopic amplitude for the all overlaps is 1. The ClustP(1) curve for the ^{16}O(^{18}O,^{16}O)^{18}O$_{2^+}$ channel was arbitrarily multiplied by 10 in order to guide the eye.

continuum states, which were not explicitly considered [44]. In the outgoing and intermediate partitions the imaginary part was scaled by a larger factor (0.78) because no couplings were introduced. This coefficient has been proved to be suitable for describing the elastic scattering cross section for many systems in a wide energy interval [45]. Woods-Saxon form factors were used to generate single and cluster wave functions. The depths of these potentials were varied to fit the experimental binding energies of both one and two neutrons. The reduced radii and diffuseness were set to 1.2 and 0.6 fm for ^{16}O and 1.26 and 0.78 fm for ^{17}O. In the case of the cluster model for the $2n + {}^{16}$O binding potential, 1.26 and 0.78 fm were also used for the reduced radius and diffuseness, respectively. The quadrupole deformation parameter $\beta = 0.355$ for the collective excitation of the ^{18}O nucleus in the entrance partition was taken from Ref. [46]. The coupling schemes used in the calculations are shown in Fig. 3.

A. Results from the cluster model

In the cluster approach, the relative motion of the two-neutron system is frozen and separated from the center of mass. In this scheme the intrinsic spin of a transferred pair of neutrons can be parallel ($S = 1$) or antiparallel ($S = 0$). The wave function of the cluster with respect to the core is determined by the principal quantum number N and the orbital angular momentum L. In transforming the wave functions of the two independent nucleons in orbits n_i, l_i into a cluster, the total number of quanta should be conserved according to the rule $\sum_{i=1}^{2} 2(n_i - 1) + l_i = 2(N - 1) + L$ [47].

As it is seen from the coupling schemes we have used in the CRC calculations, the $S = 1$ g.s. $\rightarrow$ g.s. transfer is not possible, because of parity conservation. Thus, only $S = 0$ coupling is used for the g.s. $\rightarrow$ g.s. transition. Hence, in Fig. 4 we compared the results of two calculations with the experimental data: (1) $S = 0$ for transfer from the 2^+ state of ^{18}O [ClustA(1)] and (2) $S = 1$ for the transfer from the 2^+ state [ClustP(1)]. In the first calculation the adopted spectroscopic amplitude was 1.0 for all couplings (as usually found in the literature).

For the ^{16}O(^{18}O,^{16}O)^{18}O$_{g.s.}$ channel the $S = 1$ (dashed curves in Fig. 4) calculated cross sections are lower than the $S = 0$ ones (solid curves in Fig. 4). For the ^{16}O(^{18}O,^{16}O)^{18}O$_{2^+}$ reaction the $S = 1$ cross section values are much lower than those in the experiment. To improve the quality of the figure, this last cross section was multiplied by 10. For the ^{16}O(^{18}O,^{16}O)^{18}O$_{g.s.}$ channel the $S = 0$ cross sections are noticeably larger than the experimental data for angles larger than about 25°. The $S = 0$ cross section for the ^{16}O(^{18}O,^{16}O)^{18}O$_{2^+}$ reaction is larger than the experimental data for angles larger than about 10°. One can also observe in this figure that the phase of the oscillations of the theoretical angular distributions

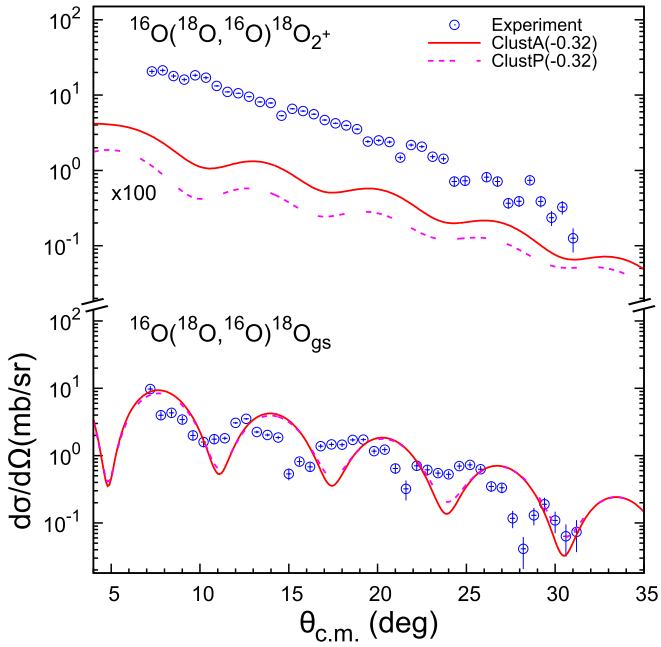


FIG. 5. Comparison of angular distributions in the cluster model in the case of the spin antiparallel [ClustA(−0.32)] and parallel [ClustP(−0.32)] transfer with the experimental data for the ^{16}O(^{18}O,^{16}O)^{18}O$_{gs}$ (bottom) and ^{16}O(^{18}O,^{16}O)^{18}O$_{2^+}$ (top) channels. The value of the spectroscopic amplitude for the 2^+ overlaps is −0.32. For a better visibility the ClustP(−0.32) calculation for the transition to the ^{18}O$_{2^+}$ state is multiplied by 100.

does not coincide with that of the experimental data for the ground state. In the case of the ^{16}O(^{18}O,^{16}O)^{18}O$_{g.s.}$ channel, the absolute value of the experimental angular distribution as well as the phase of the oscillations are better described when the total spin of the cluster in the 2^+ state of ^{18}O is $S = 1$.

A spectroscopic amplitude of −0.32 was sometimes used for the $\langle ^{18}\text{O}_{2^+} | ^{16}\text{O}_{g.s.}\rangle$ overlap in reactions with different target nuclei [19,23,24]. Therefore, it is worthwhile to compare spin parallel and antiparallel results in Fig. 4, where a spectroscopic amplitude of 1.0 is used for all overlaps, with the same calculations in Fig. 5, where the spectroscopic amplitude −0.32 is used for the 2^+ overlaps. It can be seen from Fig. 5 that a better description of the data is obtained for the ^{16}O(^{18}O,^{16}O)^{18}O$_{g.s.}$ transition. However, for the ^{16}O(^{18}O,^{16}O)^{18}O$_{2^+}$ calculations the cross sections are lower than in the experiment.

In all the present calculations, the $N = 3$, $L = 0$ configuration is used for the cluster in the ^{18}O ground state. The spectroscopic amplitude from the shell model is equal to 0.945 (see Table III below). The $N = 2$, $L = 0$ configuration with amplitude 0.241 gives a negligible contribution. Both the shape and the absolute value of the angular distribution are satisfactorily reproduced, even setting to 1.0 the spectroscopic amplitude for this configuration, as shown in Fig. 4. An amplitude of 0.92 is obtained by scaling the CRC calculated cross section to the experimental data. Negligible differences are found by extracting the amplitudes from DWBA results. This value is in good agreement with that predicted by shell-model calculations of 0.945 for a combined amplitude for $(s_{1/2})^2$ and $(d_{5/2})^2$ configurations. This result confirms the validity of the reaction model, which allows one to determine reliable spectroscopic amplitudes without the need for any arbitrary "unhappiness" factor found in the literature.

Finally, we tested the influence of some states left out of the coupling scheme shown in Fig. 3. We first included the 3^- state of the ^{16}O target. We found that its effect on the transfer cross section to the states for which there are experimental data is negligible. Second, we introduced final state interactions, i.e., the excitation of the residual nucleus (^{18}O) to the first 2^+ state and the ejectile (^{16}O) to the first 3^- state. We found the effect of the 3^- state negligible. The effect of the 2^+ state was found negligible in the transfer to the ground state. A small increment of the amplitude of the oscillations of the angular distribution corresponding to the transfer to the 2^+ state of the residual nuclei was observed. For this reason, in the calculations for the next sections, where the coupling scheme is more complicated [see Fig. 3(b)], these couplings are not considered.

B. Results from independent coordinate and two-step DWBA (CCBA)

We start from a shell-model calculation with the ZBM interaction [25] since it is rather successful in describing transfer reactions induced by ^{18}O [23]. In these calculations ^{12}C was considered as a "core" and the other nucleons moving in the valence space $1p_{1/2}$, $1d_{5/2}$, $2s_{1/2}$, described by the potential of Ref. [25]. Within this approximation, the properties of ^{18}O states are determined by the six nucleons outside the core (two protons and four neutrons).

Intermediate couplings in two-step DWBA transfer (sequential) and independent coordinate scheme calculations are important for more microscopic insight and estimation of the reaction mechanisms. To perform two-step DWBA and CRC with independent coordinate scheme calculations we use the spectroscopic amplitudes given in Tables II and III, which were obtained in Ref. [23] using the NUSHELL code [48].

We estimated the contributions of the ground state feed from ground to ground state coupling and through the intermediate 2^+ excited state of ^{18}O. To this purpose we performed the calculation by taking into account only the ground state

TABLE II. One-neutron spectroscopic amplitudes used in the two-step DWBA calculations. Here **n**, **l**, and **j** are the principal quantum number, the orbital, and the total angular momentum of the neutron orbital for one-neutron transfer [23].

One-neutron amplitudes			
Initial state/ final state	**nl$_j$**	Final state/ initial state	Spectroscopic amplitudes
^{18}O$_{g.s}(0^+)$	$1d_{5/2}$	^{17}O$_{g.s.}(5/2^+)$	+1.305
^{18}O$_{1.98}(2^+)$	$2s_{1/2}$	^{17}O$_{g.s.}(5/2^+)$	−0.929
	$1d_{5/2}$		−0.666
^{18}O$_{g.s.}(0^+)$	$2s_{1/2}$	^{17}O$_{0.87}(1/2^+)$	+0.566
^{18}O$_{g.s.}(0^+)$	$1p_{1/2}$	^{17}O$_{3.06}(1/2^-)$	−0.929
^{17}O$_{g.s.}(5/2^+)$	$1d_{5/2}$	^{16}O$_{g.s.}(0^+)$	+0.972
^{17}O$_{0.87}(1/2^+)$	$2s_{1/2}$	^{16}O$_{g.s}(0^+)$	+0.975
^{17}O$_{3.06}(1/2^-)$	$1p_{1/2}$	^{16}O$_{g.s}(0^+)$	−0.291
^{17}O$_{g.s.}(5/2^+)$	$1p_{1/2}$	^{16}O$_{6.13}(3^-)$	−0.718

TABLE III. Two-neutron spectroscopic amplitudes used in the CRC calculations. $\mathbf{n_1 l_{1j_1}}$ and $\mathbf{n_2 l_{2j_2}}$ are the principal quantum numbers, the orbital, and the total angular momenta of neutron 1 and 2 with respect to the core, and $\mathbf{J}_{12}$ is the angular momentum of two neutron system [23].

Two-neutron amplitudes				
Initial state/ final state	$\mathbf{n_1 l_{1j_1}}$ $\mathbf{n_2 l_{2j_2}}$	$\mathbf{J}_{12}$	Final state/ initial state	Spectroscopic amplitudes
$^{18}O_{g.s.}(0^+)$	$(1p_{1/2})^2$			0.241
	$(1d_{5/2})^2$	0	$^{16}O_{g.s.}(0^+)$	−0.871
	$(2s_{1/2})^2$			−0.367
$^{18}O_{1.98}(2^+)$	$(1d_{5/2})^2$	2	$^{16}O_{gs}(0^+)$	+0.641
	$1d_{5/2}2s_{1/2}$			+0.638
$^{18}O_{g.s.}(0^+)$	$1p_{1/2}1d_{5/2}$	3	$^{16}O_{6.13}(3^-)$	+0.801

to ground state coupling, first, and then by including the coupling scheme shown in Fig. 3, using both two-step DWBA approximation and CRC within the independent coordinate schemes. In both cases, a contribution of about 80% of the cross section comes from the ground state to ground state couplings. As expected this shows the one-step ground state to ground state coupling dominance, but also emphasized is the relevance of the two-step coupling processes. To check this at lower energies we have performed calculations for $E_{\rm lab} = 20$, 24, and 28 MeV. The results indicate that, even at $E_{\rm lab} = 20$ MeV, one-step transfer is still the leading reaction mechanism.

It is important to notice that throughout this work we use the nomenclature of DWBA for the two-step processes, emphasizing the fact that the coupling between different partitions is taken into account through first order DWBA. In fact as we consider the inelastic excitation in the entrance partition to high orders we should call all our two-step calculations CCBA calculations.

Also the comparison of CRC results with first order DWBA shows that higher-order couplings are around 10% of the considered couplings for the ground state to ground state transition.

The independent coordinates model for the transfer of two particles of the same mass is a model in which, in contraposition to the extreme cluster model where the internal structure of the two-neutron cluster is completely ignored, the identity of each particle is followed in detail during the transfer, although they are transferred together [49].

Comparisons of the two-step DWBA and CRC (independent coordinate) calculations with experimental data for the $^{16}O(^{18}O,^{16}O)^{18}O_{g.s.}$ and $^{16}O(^{18}O,^{16}O)^{18}O_{2^+}$ channels are shown in Fig. 6. Trends of the curves are more similar to the experimental data for both cases as compared to the cluster model calculations. For the transition to the ^{18}O ground state the two-step DWBA result is about a factor of 5 lower than the independent coordinate one. For the transition to the 2^+ state one can see from Fig. 6 that the one-step CRC calculations within the independent coordinate scheme describes the experimental angular distribution reasonably well, while the two-step DWBA calculation strongly underpredicts it (in the figure the DWBA angular distribution is multiplied by 100). A shift of angular distribution as compared to

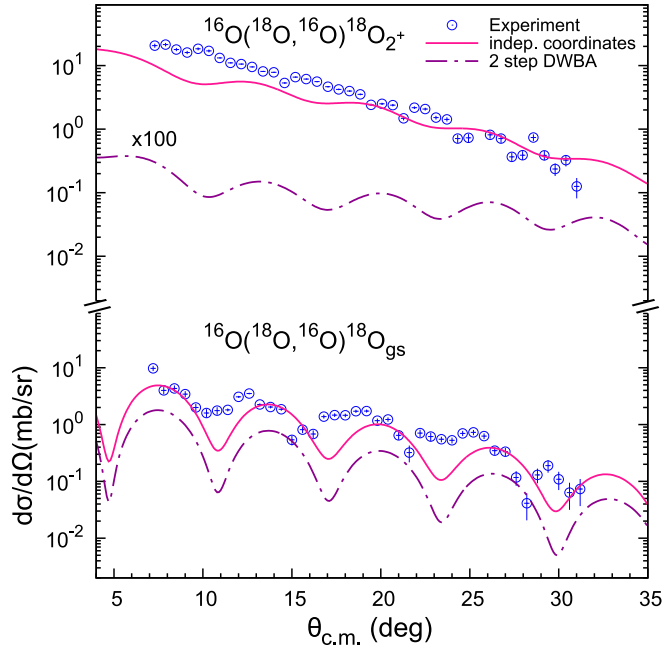


FIG. 6. Comparison of angular distributions in independent coordinate scheme and two-step DWBA transfer calculations with the experimental data for the $^{16}O(^{18}O,^{16}O)^{18}O_{gs}$ (bottom) and $^{16}O(^{18}O,^{16}O)^{18}O_{2^+}$ (top) channels. For a better visibility the two-step DWBA curve for transition to the $^{18}O_{2^+}$ state is shifted upward 100 times.

experimental data is seen in all calculations for the ground state transfer.

Until this point we performed separate calculations for the direct and sequential transfer. These two reaction mechanisms compete and they cannot be separate in the experimental observations. Therefore, we show the coherent sum of the amplitudes of these processes in Fig. 7 to see the effect of both the independent coordinate scheme and two-step DWBA transfer mechanisms. In performing the coherent sum the relative phase between one- and two-step transition amplitudes appears. The best phase was found by least χ-squared search. For the pure independent coordinate calculation $\chi^2 = 1.05$ and for the pure sequential calculation $\chi^2 = 8.2$, while for their coherent sum $\chi^2 = 0.58$ with the phase -66.7°. The improvement in the agreement is seen in both angular distribution shift and the values of cross sections.

C. Effects of the $1p_{3/2}$ and $1d_{3/2}$ orbitals

Here we perform shell-model calculations of the spectroscopic amplitudes with the psdmod interaction [26] and compare the results with the previous ZBM calculation. We consider ^{4}He as a "core" and nucleons moving in the valence space $1p_{3/2}$, $1p_{1/2}$, $1d_{5/2}$, $2s_{1/2}$, and $1d_{3/2}$ described by the potential of Ref. [26]. The results are listed in Tables IV and V. By this calculation we study the effect of newly included $1p_{3/2}$ and $1d_{3/2}$ orbitals on the reaction cross sections. Coupling schemes used in this calculation are the same as in Fig. 3.

In Fig. 8 we compare the cross sections obtained with spectroscopic amplitudes from ZBM and psdmod interactions.

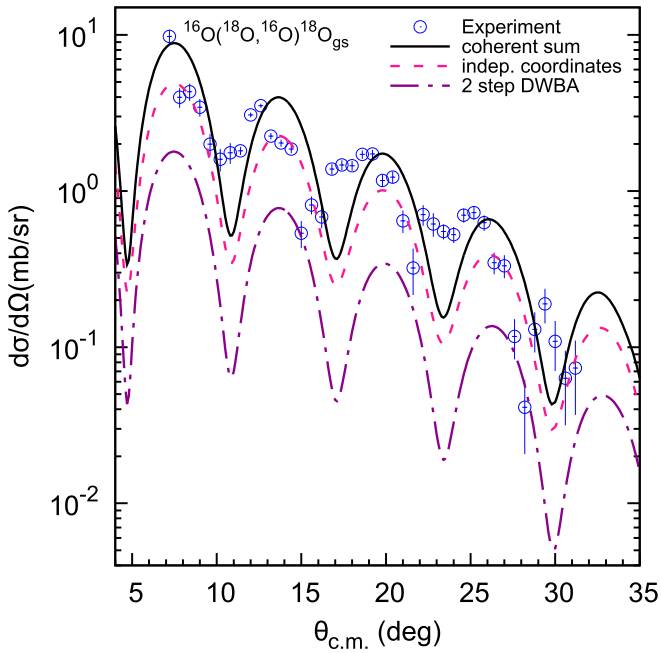


FIG. 7. Comparison of the experimental angular distributions with the coherent sum of the independent coordinate scheme and two-step DWBA calculations for the reaction ^{16}O(^{18}O ,^{16}O)^{18}O$_{g.s.}$ at 84 MeV. The spectroscopic amplitudes of Tables I and II are used.

For the independent coordinate calculation, in the case of the g.s. transition the cross section coincides while there is a factor of about 2 for the transfer to the 2+ state. No appreciable shift in the phase of the cross sections is found as compared to the ZBM calculation for both the ^{16}O(^{18}O ,^{16}O)^{18}O$_{g.s.}$ and the ^{16}O(^{18}O ,^{16}O)^{18}O$_{2^+}$ channels.

The effect of the included orbitals is more evident in the sequential transfer reaction cross section. For the ^{16}O(^{18}O ,^{16}O)^{18}O$_{g.s.}$ case the absolute values decreased by a factor of about 5 and the minima are shifted to the left

TABLE IV. One-neutron spectroscopic amplitudes obtained by psdmod interaction and used in the two-step DWBA calculations. **n**, **l**, and **j** are the principal quantum number, the orbital, and the total angular momentum of the neutron orbital for one-neutron transfer.

One-neutron amplitudes			
Initial state/ final state	**nl$_j$**	Final state/ initial state	Spectroscopic amplitudes
^{18}O$_{g.s.}$(0$^+$)	$1d_{5/2}$	^{17}O$_{g.s.}$(5/2$^+$)	+1.272
	$2s_{1/2}$		+0.495
^{18}O$_{1.98}$(2$^+$)	$1d_{3/2}$	^{17}O$_{g.s.}$(5/2$^+$)	+0.081
	$1d_{5/2}$		+1.111
^{18}O$_{g.s.}$(0$^+$)	$2s_{1/2}$	^{17}O$_{0.87}$(1/2$^+$)	+0.445
^{18}O$_{g.s.}$(0$^+$)	$1p_{1/2}$	^{17}O$_{3.06}$(1/2$^-$)	+0.845
^{17}O$_{g.s.}$(5/2$^+$)	$1d_{5/2}$	^{16}O$_{g.s.}$(0$^+$)	+0.957
^{17}O$_{0.87}$(1/2$^+$)	$2s_{1/2}$	^{16}O$_{g.s.}$(0$^+$)	+0.973
^{17}O$_{3.06}$(1/2$^-$)	$1p_{1/2}$	^{16}O$_{g.s.}$(0$^+$)	−0.239
^{17}O$_{g.s.}$(5/2$^+$)	$1p_{1/2}$	^{16}O$_{6.13}$(3$^-$)	−0.620
	$1p_{3/2}$		+0.194

TABLE V. Two-neutron spectroscopic amplitudes obtained by psdmod interaction and used in the CRC calculations. $\mathbf{n_1l_{j_1}}$ and $\mathbf{n_2l_{2_{j_2}}}$ are the principal quantum numbers, the orbital, and the total angular momenta of neutron 1 and 2 with respect to the core, and $\mathbf{J}_{12}$ is the angular momentum of the two-neutron system.

Two-neutron amplitudes				
Initial state/ final state	$\mathbf{n_1l_{1_{j_1}}}$ $\mathbf{n_2l_{2_{j_2}}}$	$\mathbf{J}_{12}$	Final state/ initial state	Spectroscopic amplitudes
	$(1p_{1/2})^2$			+0.142
	$(1d_{5/2})^2$			−0.857
^{18}O$_{g.s.}$(0$^+$)	$(1d_{3/2})^2$	0	^{16}O$_{g.s.}$(0$^+$)	−0.191
	$(2s_{1/2})^2$			−0.308
	$(1p_{3/2})^2$			+0.045
	$(1d_{5/2})^2$			+0.756
	$1d_{5/2}1d_{3/2}$			−0.079
	$1d_{5/2}2s_{1/2}$			+0.475
^{18}O$_{1.98}$(2$^+$)	$1(d_{3/2})^2$	2	^{16}O$_{g.s.}$(0$^+$)	+0.107
	$1d_{3/2}2s_{1/2}$			+0.171
	$1(p_{3/2})^2$			+0.014
	$1p_{3/2}1p_{1/2}$			+0.011
	$1p_{1/2}1d_{5/2}$			+0.715
^{18}O$_{g.s.}$(0$^+$)	$1p_{3/2}1d_{5/2}$	3	^{16}O$_{6.13}$(3$^-$)	+0.235
	$1p_{3/2}1d_{3/2}$			−0.089

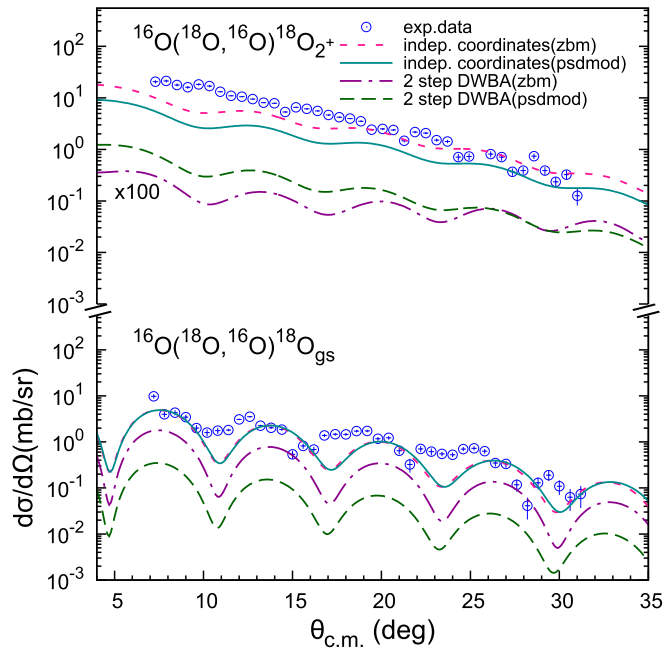


FIG. 8. Comparison of the angular distributions in the independent coordinate scheme and two-step DWBA transfer calculations with the spectroscopic amplitudes obtained by ZBM interaction and those obtained by psdmod interaction for the ^{16}O(^{18}O ,^{16}O)^{18}O$_{g.s.}$ (bottom) and ^{16}O(^{18}O ,^{16}O)^{18}O$_{2^+}$ (top) channels. The two-step DWBA curve, derived using the ZBM spectroscopic amplitudes, for the ^{16}O(^{18}O ,^{16}O)^{18}O$_{2^+}$ channel was arbitrarily multiplied by 100 in order to guide the eye.

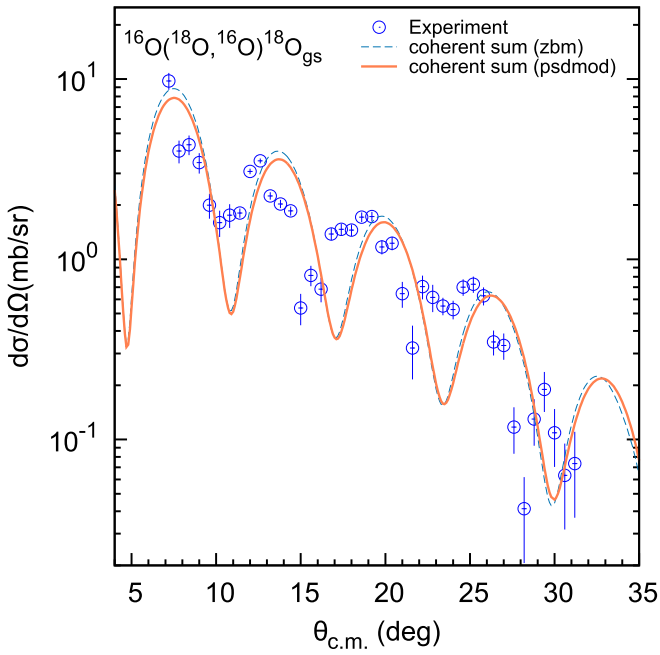


FIG. 9. Comparison of the experimental angular distributions with the coherent sum of independent coordinates and the two-step DWBA calculations for the reaction ^{16}O(^{18}O,^{16}O)^{18}O$_{gs}$ at 84 MeV. The spectroscopic amplitudes of Tables I and II, III, and IV are used.

by about 0.1° at the largest angles. The ^{16}O(^{18}O,^{16}O)^{18}O$_{2^+}$ cross section is increased around 200 times as compared to the ZBM calculation and the shift of minima is about 0.1° as in the ground state case.

For completeness we show the comparison of a coherent sum of sequential transfer and independent scheme cross sections in ZBM and psdmod calculations in Fig. 9. Here also an arbitrary phase appears in performing the coherent sum. We have found the phase which corresponds to the least χ^2 as in the case of the ZBM calculation. Although the coherent sum of independent coordinates and the two-step DWBA approximation with psdmod calculation ($\chi^2 = 0.59$ with phase $-0.3°$) is improved as compared to the pure independent coordinates calculation ($\chi^2 = 1.09$), it is almost not changed as compared to the coherent sum of independent coordinates and the two-step DWBA approximation with ZBM calculation ($\chi^2 = 0.58$).

IV. CONCLUSIONS

In this work we have analyzed both experimental and theoretical aspects of the two-neutron transfer reaction in ^{16}O(^{18}O,^{16}O)^{18}O. Broad conclusions from the investigation conducted are as follows:

(1) The one-step reaction mechanism is dominant and the transfer of correlated nucleons mostly takes place through the spin antiparallel condition.
(2) The theoretical analysis shows that at the bombarding energy considered in this work and in the range of angles where the experimental data were measured, the reaction mainly goes through the elastic transfer of nucleons rather than elastic scattering of the projectile, though in the experiment elastic scattering of a projectile at a given θ is indistinguishable from the elastic transfer at the angle $\pi - \theta$.
(3) The CRC calculations within the independent coordinate scheme better describe the data compared to the extreme cluster model. This is an expected result since the independent coordinate scheme accounts for a larger set of configurations in the truncated shell-model space. However, the cluster model gives an acceptable description of the ground state to ground state transition, similarly to what was found in Ref. [23]. This allows one to conclude that a large component ($S = 0$) of the ^{18}O ground state wave function is clusterized in a two-neutron pair with cluster quantum numbers $N = 3$, $L = 0$ compared to the ^{16}O$_{0^+}$ core.
(4) The spectroscopic factors obtained by the inclusion of $1p_{3/2}$ and $1d_{3/2}$ orbitals mainly affect the sequential mechanism.
(5) The interplay between the transfer of the two neutrons and the excited states of the counterparts have a sizable impact in the final cross sections.

ACKNOWLEDGMENTS

M.J.E. acknowledges support from a TWAS-CNPq grant and Grant No. F2-FA-F177 of the Uzbekistan Academy of Sciences. The Brazilian authors acknowledge the partial support from CNPq and CAPES. The research leading to these results received funding from the European Commission, Seventh Framework Program (FP7/2007-2013) under Grant Agreement No. 600376. J.A.L. is supported by a Marie Curie Piscopia fellowship at the University of Padova.

[1] G. R. Satchler, *Direct Nuclear Reactions* (Oxford University Press, New York, 1983).
[2] R. Broglia and A. Winther, *Heavy Ion Reactions: The Elementary Processes*, Frontiers in Physics (Addison-Wesley, Reading, MA, 1991).
[3] M. A. Rahman and M. S. Chowdhury, Phys. Rev. C **73**, 054311 (2006).
[4] M. S. Golovkov, L. V. Grigorenko, A. S. Fomichev, S. A. Krupko, Y. T. Oganessian, A. M. Rodin, S. I. Sidorchuk, R. S. Slepnev, S. V. Stepantsov, G. M. Ter-Akopian, R. Wolski, M. G. Itkis, A. S. Denikin, A. A. Bogatchev, N. A. Kondratiev, E. M. Kozulin, A. A. Korsheninnikov, E. Y. Nikolskii, P. Roussel-Chomaz, W. Mittig, R. Palit, V. Bouchat, V. Kinnard, T. Materna, F. Hanappe, O. Dorvaux, L. Stuttgé, C. Angulo, V. Lapoux, R. Raabe, L. Nalpas, A. A. Yukhimchuk, V. V. Perevozchikov, Y. I. Vinogradov, S. K. Grishechkin, and S. V. Zlatoustovskiy, Phys. Rev. C **72**, 064612 (2005).
[5] M. A. Rahman and M. S. Chowdhury, Phys. Rev. C **72**, 054303 (2005).
[6] M. S. Golovkov, L. V. Grigorenko, A. S. Fomichev, S. A. Krupko, Y. T. Oganessian, A. M. Rodin, S. I. Sidorchuk, R. S. Slepnev, S. V. Stepantsov, G. M. Ter-Akopian, R. Wolski,

M. G. Itkis, A. A. Bogatchev, N. A. Kondratiev, E. M. Kozulin, A. A. Korsheninnikov, E. Y. Nikolskii, P. Roussel-Chomaz, W. Mittig, R. Palit, V. Bouchat, V. Kinnard, T. Materna, F. Hanappe, O. Dorvaux, L. Stuttgé, V. Lapoux, R. Raabe, L. Nalpas, A. A. Yukhimchuk, C. Angulo, V. V. Perevozchikov, Y. I. Vinogradov, S. K. Grishechkin, and S. V. Zlatoustovskiy, Phys. Rev. Lett. **93**, 262501 (2004).

[7] M. Golovkov, Y. Oganessian, D. Bogdanov, A. Fomichev, A. Rodin, S. Sidorchuk, R. Slepnev, S. Stepantsov, G. Ter-Akopian, R. Wolski, V. Gorshkov, M. Chelnokov, M. Itkis, E. Kozulin, A. Bogatchev, N. Kondratiev, I. Korzyukov, A. Yukhimchuk, V. Perevozchikov, Y. Vinogradov, S. Grishechkin, A. Demin, S. Zlatoustovskiy, A. Kuryakin, S. Fil'chagin, R. Il'kayev, F. Hanappe, T. Materna, L. Stuttge, A. Ninane, A. Korsheninnikov, E. Nikolskii, I. Tanihata, P. Roussel-Chomaz, W. Mittig, N. Alamanos, V. Lapoux, E. Pollacco, and L. Nalpas, Phys. Lett. B **566**, 70 (2003).

[8] M. B. Becha, C. O. Blyth, C. N. Pinder, N. M. Clarke, R. P. Ward, P. R. Hayes, K. I. Pearce, D. L. Watson, A. Ghazarian, M. D. Cohler, I. J. Thompson, and M. A. Nagarajan, Phys. Rev. C **56**, 1960 (1997).

[9] P. Guazzoni, M. Jaskola, L. Zetta, A. Covello, A. Gargano, Y. Eisermann, G. Graw, R. Hertenberger, A. Metz, F. Nuoffer, and G. Staudt, Phys. Rev. C **60**, 054603 (1999).

[10] P. Guazzoni, L. Zetta, A. Covello, A. Gargano, G. Graw, R. Hertenberger, H.-F. Wirth, and M. Jaskola, Phys. Rev. C **69**, 024619 (2004).

[11] P. Guazzoni, L. Zetta, A. Covello, A. Gargano, B. F. Bayman, G. Graw, R. Hertenberger, H.-F. Wirth, and M. Jaskola, Phys. Rev. C **74**, 054605 (2006).

[12] P. Guazzoni, L. Zetta, A. Covello, A. Gargano, B. F. Bayman, T. Faestermann, G. Graw, R. Hertenberger, H.-F. Wirth, and M. Jaskola, Phys. Rev. C **78**, 064608 (2008).

[13] P. Guazzoni, L. Zetta, A. Covello, A. Gargano, B. F. Bayman, T. Faestermann, G. Graw, R. Hertenberger, H.-F. Wirth, and M. Jaskola, Phys. Rev. C **83**, 044614 (2011).

[14] G. Potel, F. Barranco, F. Marini, A. Idini, E. Vigezzi, and R. A. Broglia, Phys. Rev. Lett. **107**, 092501 (2011).

[15] G. Potel, F. Barranco, E. Vigezzi, and R. A. Broglia, Phys. Rev. Lett. **105**, 172502 (2010).

[16] G. Potel, F. Barranco, F. Marini, A. Idini, E. Vigezzi, and R. A. Broglia, Phys. Rev. Lett. **108**, 069904(E) (2012).

[17] G. Potel, A. Idini, F. Barranco, E. Vigezzi, and R. A. Broglia, Rep. Prog. Phys. **76**, 106301 (2013).

[18] P. D. Bond, H. J. Korner, M. C. Lemaire, D. J. Pisano, and C. E. Thorn, Phys. Rev. C **16**, 177 (1977).

[19] M.-C. Lemaire and K. S. Low, Phys. Rev. C **16**, 183 (1977).

[20] F. Cappuzzello, D. Carbone, M. Cavallaro, M. Bondì, C. Agodi, F. Azaiez, A. Bonaccorso, A. Cunsolo, L. Fortunato, A. Foti *et al.*, Nat. Commun. **6**, 6743 (2015).

[21] F. Cappuzzello, C. Rea, A. Bonaccorso, M. Bondì, D. Carbone, M. Cavallaro, A. Cunsolo, A. Foti, S. Orrigo, M. Rodrigues, and G. Taranto, Phys. Lett. B **711**, 347 (2012).

[22] D. Carbone, M. Bondì, A. Bonaccorso, C. Agodi, F. Cappuzzello, M. Cavallaro, R. J. Charity, A. Cunsolo, M. De Napoli, and A. Foti, Phys. Rev. C **90**, 064621 (2014).

[23] M. Cavallaro, F. Cappuzzello, M. Bondì, D. Carbone, V. N. Garcia, A. Gargano, S. M. Lenzi, J. Lubian, C. Agodi, F. Azaiez, M. De Napoli, A. Foti, S. Franchoo, R. Linares, D. Nicolosi, M. Niikura, J. A. Scarpaci, and S. Tropea, Phys. Rev. C **88**, 054601 (2013).

[24] A. Parmar, Sonika, B. Roy, V. Jha, U. Pal, T. Sinha, S. Pandit, V. Parkar, K. Ramachandran, K. Mahata, S. Santra, and A. Mohanty, Nucl. Phys. A **940**, 167 (2015).

[25] A. P. Zuker, B. Buck, and J. B. McGrory, Phys. Rev. Lett. **21**, 39 (1968).

[26] Y. Utsuno and S. Chiba, Phys. Rev. C **83**, 021301 (2011).

[27] E. K. Warburton and B. A. Brown, Phys. Rev. C **46**, 923 (1992).

[28] F. Cappuzzello, D. Carbone, M. Cavallaro, and A. Cunsolo, in *Magnets: Types, Uses, and Safety* (Nova Science Publishers, New York, 2011), p. 163.

[29] M. Cavallaro, F. Cappuzzello, A. Cunsolo, A. Foti, and D. Carbone, AIP Conf. Proc. **1213**, 198 (2010).

[30] F. Cappuzzello, C. Agodi, D. Carbone, and M. Cavallaro, Eur. Phys. J. A **52**, 167 (2016).

[31] M. Cavallaro, F. Cappuzzello, D. Carbone, A. Cunsolo, A. Foti, A. Khouaja, M. R. D. Rodrigues, J. S. Winfield, and M. Bondì, Euro. Phys. J. A **48**, 59 (2012).

[32] F. Cappuzzello, M. Cavallaro, A. Cunsolo, A. Foti, D. Carbone, S. Orrigo, and M. Rodrigues, Nucl. Instrum. Methods Phys. Res. Sect. A **621**, 419 (2010).

[33] F. Cappuzzello, D. Carbone, and M. Cavallaro, Nucl. Instrum. Methods Phys. Res. Sect. A **638**, 74 (2011).

[34] M. Cavallaro, F. Cappuzzello, D. Carbone, A. Cunsolo, A. Foti, and R. Linares, Nucl. Instrum. Methods Phys. Res. Sect. A **637**, 77 (2011).

[35] D. Carbone, Eur. Phys. J. Plus **130**, 143 (2015).

[36] J. F. Ziegler, M. D. Ziegler, and J. P. Biersack, SRIM: The stopping and range of ions in matter, version 2008.04, http://www.srim.org/

[37] M. E. Cobern, L. C. Bland, H. T. Fortune, G. E. Moore, S. Mordechai, and R. Middleton, Phys. Rev. C **23**, 2387 (1981).

[38] M. Cavallaro, F. Cappuzzello, D. Carbone, A. Cunsolo, A. Foti, R. Linares, D. Pereira, J. Oliveira, P. Gomes, J. Lubian, and R. Chen, Nucl. Instrum. Methods Phys. Res., Sect. A **648**, 46 (2011).

[39] A. Vitturi and C. Dasso, Nucl. Phys. A **458**, 157 (1986).

[40] J. Christley, M. Nagarajan, and A. Vitturi, Nucl. Phys. A **591**, 341 (1995).

[41] O. Akyuz and A. Whinther, in *Proceedings of the Enrico Fermi Summer School in Physics*, edited by R. A. Broglia, C. H. Dasso, and R. A. Ricci (North Holland, Amsterdam, 1981).

[42] I. A. Thompson, www.fresco.org.uk.

[43] L. C. Chamon, B. V. Carlson, L. R. Gasques, D. Pereira, C. De Conti, M. A. G. Alvarez, M. S. Hussein, M. A. Cândido Ribeiro, E. S. Rossi, and C. P. Silva, Phys. Rev. C **66**, 014610 (2002).

[44] D. Pereira, J. Lubian, J. Oliveira, D. de Sousa, and L. Chamon, Phys. Lett. B **670**, 330 (2009).

[45] L. Gasques, L. Chamon, P. Gomes, and J. Lubian, Nucl. Phys. A **764**, 135 (2006).

[46] S. Raman, C. W. Nestor, Jr., and P. Tikkanen, At. Data Nucl. Data Tables **78**, 1 (2001).

[47] M. Moshinsky, Nucl. Phys. **13**, 104 (1959).

[48] NUSHELL for Windows and Linux, http://www.garsington.eclipse.co.uk/

[49] I. J. Thompson, Comput. Phys. Rep. **7**, 167 (1988).